Available online at www.sciencedirect.com

SCIENCE DIRECT

Thin Solid Films 484 (2005) 426 – 432

www.elsevier.com/locate/tsf

A tensile-testing technique for micrometer-sized free-standing thin films☆

Yi-Wen Cheng*, David T. Read, J. David McColskey, Joyce E. Wright

National Institute of Standards and Technology, Boulder, CO 80305-3328, USA

Received 12 March 2004; received in revised form 9 February 2005; accepted 11 March 2005
Available online 17 May 2005

Abstract

A tensile-testing technique for micrometer-sized free-standing thin films is described and sample results obtained using the technique are presented. Major components used in the technique include a three-axis micromanipulator, a force sensor, two desktop computers, and a microscope. The design and fabrication of specimens by use of microfabrication methods are an integral part of the technique because they are crucial for testing to be successful. The micromanipulator is computer-controlled and has a speed range from 0.004 to 2 μm/s in each axis. The force sensor is an eddy-current device and has force capacities in millinewtons. The desktop computers are used to control the micromanipulator, and to acquire data and images, which are used to calculate strains with a digital-image-correlation technique. The nominal dimension of a typical specimen is 180 μm × 10 μm × 1 μm and tests can be conducted from ambient temperature (~23 °C) to 200 °C. Over the last few years, the technique has been successfully used in our laboratory to test polysilicon, pure aluminum, aluminum alloys, photodefinable polyimide, and electrodeposited copper.

Keywords: Aluminum; Copper; Mechanical properties; Thin-film mechanical test

1. Introduction

Tensile tests provide properties of Young's modulus, strength, and ductility of materials under uniaxial tensile loadings. These properties are often specified for a given material and used for comparison of materials, development of new materials, and quality control. In addition, tensile properties are the essential input parameters for structural design, numerical modeling and simulation of mechanical behavior of materials in structures.

Tensile properties are generally measured with procedures in accordance with standard tensile-test methods, such as ASTM E8, ASTM E8M, and ASTM E345 [1–3]. Specimens used in these test methods are typically several millimeters or even centimeters in thickness for rectangular specimens, or in diameter for round specimens, which are a few orders of magnitude larger than thin films used in today's microelectronics industry. Unfortunately, the testing machines, gripping devices, and specimen-preparation procedures prescribed in the standard test methods are difficult to apply in testing thin films that have thicknesses measured in micrometers or submicrometers.

Micrometer- or submicrometer-sized thin films typically have microstructures and properties, which are influenced by their fabrication processes, that are different from bulk materials of the same nominal chemical composition [4]. Extrapolations of properties of films prepared by one process often cannot be made from films prepared by another process or from bulk specimens. The properties of thin films need to be measured in the dimension and conditions that are used in actual structural applications.

To measure tensile properties of thin films, researchers have developed various techniques. Early developments of the experimental techniques have been reviewed by Hoffman [5], and Menter and Pashley [6]. Most of the specimens used in these early approaches are still relatively large compared with those of current interest. Specimen fabrication, preparation, and especially mounting specimens to the

☆ Contribution of NIST, an agency of the U.S. Government; not subject to copyright.

* Corresponding author.
E-mail address: cheng@boulder.nist.gov (Y.-W. Cheng).

0040-6090/$ - see front matter © 2005 Elsevier B.V. All rights reserved.
doi:10.1016/j.tsf.2005.03.030

loading devices were cited to be the major difficulties for the early-developed techniques.

Recent developments in the test methods for thin films use microfabrication techniques, including lithography, deposition, and etching, to produce micrometer-sized tensile specimens [7–13]. Microfabrication techniques offer the following advantages:

i. A large number of specimens with uniform thickness, composition, geometry, and structure are fabricated in a single process run.
ii. Tensile tests can be conducted with as-fabricated as well as heat-treated specimens, which are easy to handle and test.

Different specimen-gripping and -loading methods have been used by different researchers, such as electrostatic [8,11] or direct pin-like [13] grippings. Different techniques also have been used to obtain the real specimen strains, such as image correlation [9,13] or using different specimen lengths to correct for load-train compliance [7].

Other indirect methods, such as the instrumented indentation test [14] and the bulge test [15], have also been used to derive the properties of Young's modulus and strengths of the material. This paper describes a tensile-testing technique, including specimen fabrication, that has been used to test micrometer-sized free-standing tensile specimens in our laboratory over the last few years.

2. Specimen design and fabrication

Microfabrication techniques similar to those used in the semiconductor industry are used to fabricate the test specimens. The substrates are (100) silicon wafers coated by suppliers with a "wet" oxide layer about 0.5 μm thick. Depending on the material to be tested and the deposition processes used, the pattern-and-etch steps vary. Here, we describe three different specimen-preparation procedures. A typical fabricated specimen ready for testing is shown in Fig. 1.

2.1. Specimen 1: electron-beam (EB) physical-vapor-deposited (PVD) 99.999% aluminum [13,16]

A mask-pattern-etch procedure was used to produce a rectangular window, the darker area shown in Fig. 1, where the specimen resides. The silicon oxide within the window was then etched and removed with diluted hydrofluoric acid (HF) to expose the underlying bare silicon. Pure aluminum (99.999%) was evaporated by EB in a base vacuum of 1.3×10^{-4} Pa and condensed on the etched silicon wafer held on a water-cooled mount.

The specimen was formed on bare silicon by subtractive photolithography using masking and wet-chemical etching. One end of the specimen's gauge section (right side in Fig. 1) connects to the surrounding film that is on the oxide. The other end connects to a tab, which has a 50 μm hole for pin-loading. There are three tethers connected to the tab, as shown in Fig. 1. The gauge section, the tab, and the tethers were then freed by chemically removing the underlying silicon substrate with xenon difluoride (XeF_2). For easy loading, the silicon needs to be removed to a depth of at least 50 μm. The function of the tethers is to hold the tab in place after the underlying silicon has been removed.

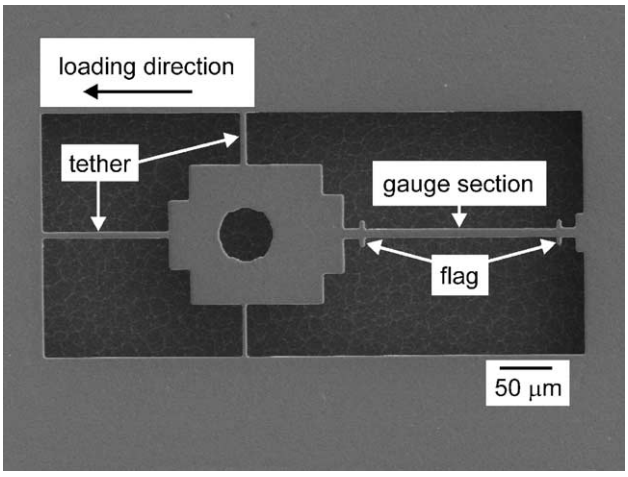

Fig. 1. A typical specimen ready for testing. The specimen has been etched with XeF_2. The large, circular hole at the middle of the tab is for loading with a tungsten hook.

The original design [13] for the loading hole was a square because it was more convenient for the mask-design software to generate. During testing, however, failure commonly occurred at the loading hole with cracks initiated at the corners of the hole. The current specimen has a circular hole that eliminates the loading-hole failure. At the ends of the gauge section, there are flags that facilitate the measurements of displacement and strain by the image-correlation technique [17,18].

The nominal dimension for the gauge section of the rectangular specimen is 180 μm × 10 μm × 1 μm. For stress and strain calculations, the dimension of each specimen is individually measured. The thickness was determined by a profilometer. The length and width were measured with a scanning electron microscope (SEM). The measurement accuracy of length and width is within ±1%, while thickness is within ±3%.

2.2. Specimen 2: photodefinable polyimide [19]

The general specimen-fabrication and XeF_2-etching procedures were the same as those used for fabrication of Specimen 1. For fabrication of Specimen 2, a commercial photodefinable polyimide was spin-coated on the patterned-and-etched silicon wafer. Specimens were formed by photolithography by use of masking and etching, and then cured at 380 °C in a nitrogen environment.

2.3. Specimen 3: electrochemically deposited copper

The silicon-oxide layer on the wafer was removed with HF. A 60 nm layer of evaporated copper was deposited onto the bare silicon to function as a seed layer for subsequent electrochemical deposition. Specimens were formed with photolithographic procedures similar to those used for Specimen 1. Electrochemical deposition using a copper-sulfate bath was subsequently used to deposit a copper layer of thickness 2.53 μm on the patterned-and-etched silicon wafer. Only the area that was electrically conductive received the copper deposit. The deposited wafer was subsequently etched by XeF_2.

3. Test apparatus

The test apparatus consists of the following components:

i. A moving stage consisting of a three-axis micromanipulator, which is controlled by a desktop computer, is used to apply force, and to handle and position the specimen. As quoted from the manufacturer [20], the micromanipulator assembly has a travel range of 25 mm in each axis. The motor drive for each axis has an encoder of 0.05 μm resolution that determines the resolution of stage movement. The motor has a speed range from 0.004 to 2 μm/s. It is noted that the manufacturer's specifications of the micromanipulators given here are for reference only. The actual strains of a specimen during a test are determined from the acquired images of specimen surface.

ii. A force sensor with a loading assembly, which is attached to the micromanipulator assembly as shown in Fig. 2, is used to measure the force applied to the specimen during a test. The force sensor contains an eddy-current displacement sensor and two steel flex strips. As shown in the figure, the ends of the steel strips are screw-fastened to two ceramic blocks that serve as a heat insulator when tests are performed at elevated temperatures. The top ceramic block is attached to the micromanipulator assembly and the bottom one is free to move with the flex strips. A brass loading bar with a tungsten hook at its end is attached to the bottom ceramic block. The brass bar is aligned to one of the micromanipulator's axes to facilitate loading alignment during testing. The tungsten hook is a wafer probe with its tip blunted and bent for easy and secure hooking to the specimen.
The steel strips have a fixed nominal length of 20.3 mm and a width of 6.4 mm. Two thicknesses, 0.13 mm and 0.38 mm, have been used depending on load requirements.

iii. Two desktop computers, which are equipped with data-acquisition, instrument-control, and image-capture devices, are used for controlling the micromanipulator, acquiring data on force and movement of the moving stage, and acquiring images of specimen's surface during testing. Our current setup uses the first computer for controlling the micromanipulator and acquiring data on force and stage movement. The second computer acquires images of specimen's surface during testing. The two computers are synchronized through communications via serial ports on the computers, so that the data on force and stage movement correspond with the images taken at the same time.

iv. An optical microscope equipped with a digital camera is used for magnification and for providing specimen's images. High magnification is needed to view the specimen during loading preparation and loading alignment. The images of specimen's surface throughout a test are required for calculation of specimen's extensions and strains. For the microscope with a 10× eyepiece, we use 2.25× and 8× objective lenses for handling specimens during loading preparation and 25× for images during loading. Because the loading assembly is under the lenses during loading preparation and actual loading, a microscope of relatively long focal length is required to provide adequate space between the lens and the specimen. For our 25× lens, the focal length is about 20 mm. We also conducted tests in SEM, which has continuous magnifications that provide sufficient flexibility for handling and testing specimens.

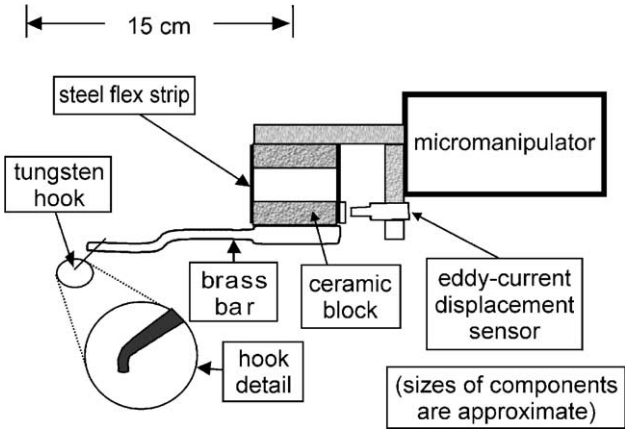

Fig. 2. Schematic of loading device and force sensor.

4. Force-sensor calibration

In reference to Fig. 3, a vertical through-hole is drilled near the end of the brass bar. A pendulum is set up with a string held stationary at the top and a known weight hanging at the bottom. The string is placed in a position so that it

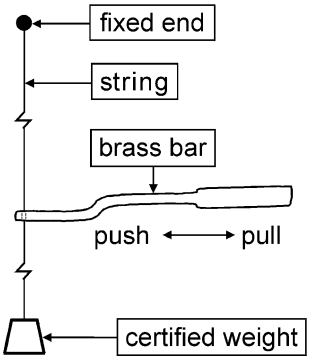

Fig. 3. Setup for force-sensor calibration. The brass bar is attached to a micromanipulator as shown in Fig. 2.

passes through the hole without touching the sidewall of the hole. The sidewall is smoothed to minimize friction between the string and the sidewall when the bar is moved against the string.

The micromanipulator as shown in Fig. 2 is moved in the direction in the same manner as during a test. Depending on the direction of the micromanipulator's motion, the brass bar will pull or push the string and deflect the steel strips (see Fig. 2). This changes the gap between the eddy-current displacement sensor and the steel-strip assembly, causing sensor outputs in voltage to change in proportion to the gap distance. From the weight, the sensor outputs, and the string length between the fixed point and the string-bar contact point, we obtain a force-versus-voltage calibration plot, as shown in Fig. 4.

Calibration is performed periodically. Five identical runs (cycles) are typically performed and each run produces one force–voltage proportional value (7.068 in Fig. 4). The average of the five force–voltage proportional values is

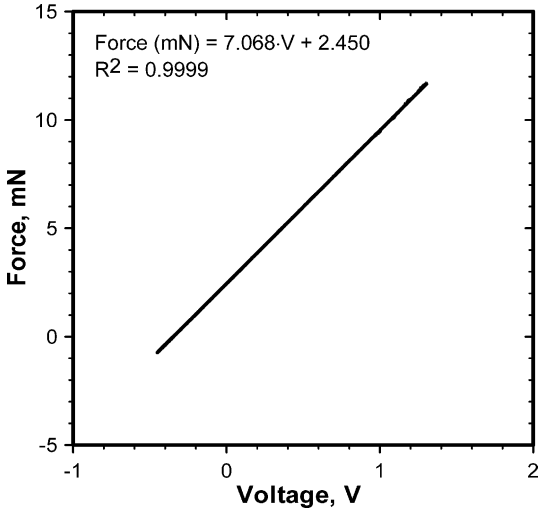

Fig. 4. Force-sensor calibration plot for strips 0.13 mm thick. The apparent linear line of the plot is comprised of actual data points of one cycle of measurements, that is from −0.44 V to 1.28 V and then back to −0.44 V, and the linear-regression line drawn through the data points. R is the linear regression coefficient.

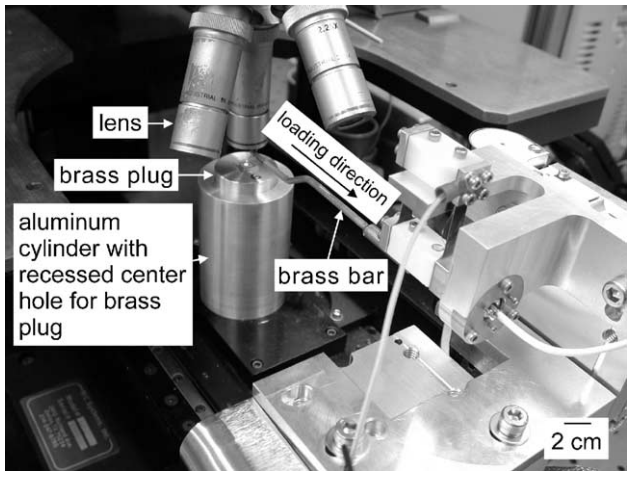

Fig. 5. Photographic view of the test fixture. The chip containing specimens is just below the middle lens.

used for subsequent force calculations. At the 95% confidence level, the uncertainty in the calibration factor is about ±1%. Three micromanipulator's travel speeds, 1, 10, and 100 μm/s, have been used to determine any possible effects of velocity. No effect was observed for the range tested.

5. Measurements of specimen's extension and strain

Measurements of extension and strain of the micrometer-sized specimens over the gauge length are difficult to make by means of small scribe lines or marks, or by a clip-on extensometer. While laser interferometry has been used [21] to directly measure the specimen's extension during a test, we use the digital image-correlation technique [17,18] to calculate the extension and the strain. The strain is calculated by dividing the relative movement between the two flags (see Fig. 1), measured with the image-correlation technique, by the original gauge length. The resolution of the image-correlation technique we use is 0.02 pixels. With a specimen magnified 350 times, which is the typical magnification we have been using in the tests, 0.02 pixels is equivalent to 0.01 μm in length or 55.6 microstrain with a gauge length of 180 μm. The resolution improves with higher magnifications. The strain rate of a test is calculated using the difference in strain values at the beginning of the test

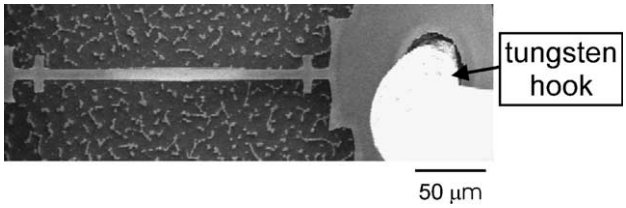

Fig. 6. SEM image of a specimen ready for testing with tungsten hook engaged in the loading hole.

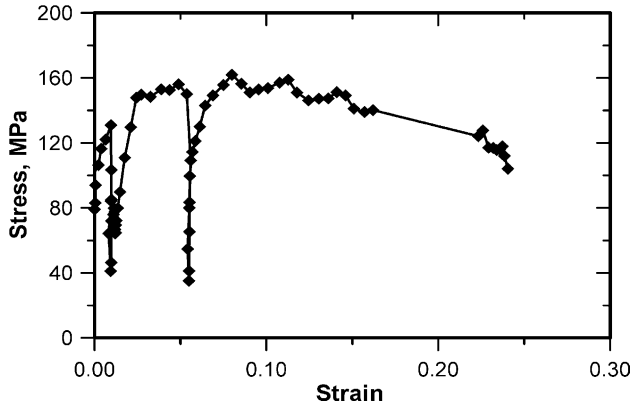

Fig. 7. Stress–strain curve with two unloading–reloading cycles, which are occasionally performed to provide additional measurements for Young's modulus. Material: EB-PVD aluminum.

and at the maximum load divided by the corresponding elapsed time between these two points.

6. Preparation and test

The wafer, containing specimens that are prepared as described in Section 2, is usually cut into chips approximately 1×1 cm^2. Typically, each chip has 24 specimens. The chip, which is under the middle lens shown in Fig. 5, is laid flat and glued onto a brass plug with silver paint.

To align the specimen's gauge section to the loading axis, we adjust the brass bar with the micromanipulator to a position so that the tungsten-probe tip is just a few micrometers above the chip's top surface. The orientation of the specimen's gauge section is then hand-adjusted with rotation of the aluminum cylinder to align with the movement of the brass bar when the bar moves along the loading direction, just as in an actual tensile test.

Table 1
Test results for polyimide specimens: 0.2% offset yield strength (YS), UTS, slope of the linear part of stress–strain curve, and elongation to failure

	YS, MPa	UTS, MPa	Slope, GPa	Elongation, %
	114	180	5.6	22
	120	171	5.1	22
	94	184	5.7	22
	89	182	5.8	23
	96	181	5.6	23
	90	178	5.8	23
	100	177	4.3	24
	108	185	5.8	25
	102	182	5.6	23
	108	185	5.7	26
	110	186	5.3	27
Average	103	181	5.5	24
Standard deviation	10	4.4	0.4	1.6
Manufacturer's data [23]	Not available	178	4.7	>10

Tests were conducted at ambient temperature (~23 °C) and an average strain rate of 7.1×10^{-4} s^{-1}.

Table 2
Results for polyimide at elevated temperatures and an average strain rate of 7.1×10^{-4} s^{-1}

Temperature, °C	YS, MPa	UTS, MPa	Slope, GPa	Elongation, %
80	95	146	4.9	19
150	64	118	3.6	22
150	59	118	3.5	27
200	50	93	2.0	31
200	52	91	2.6	27

After the tethers are severed with the tungsten hook, the hook is moved to engage with the specimen's loading hole, as shown in Fig. 6. With the desired testing speed selected and image quality adjusted, the specimen is pulled with the computer-controlled micromanipulator. During the test, force signals, displacements of the loading stage, and images of the specimen surface are acquired and stored for analyses.

7. Tests at elevated temperatures

For tests at elevated temperatures, the brass plug (see Fig. 5) is set on a ceramic block serving as a heat insulator. Heating elements are embedded inside the plug just beneath the top surface. A type K thermocouple is attached adjacent to the chip. Heating elements are also used to wrap around the brass bar at the tungsten-hook end.

In addition to monitoring and controlling at the plug, temperature is also monitored at the junction of the tungsten probe and the brass bar with a type K thermocouple. With this setup, we can test specimens from ambient temperature (~23 °C) to 200 °C. The drawback of the current setup is that the temperature of the specimen is not directly monitored. We have not measured the temperature difference between the specimen and the two monitoring thermocouples.

8. Sample results

Fig. 7 shows an example stress–strain plot for EB-PVD aluminum (Specimen 1) tested at ambient temperature (~23 °C). From the plot, using the procedures described in the testing standards [1,2] we can determine the 0.2% offset yield strength, the ultimate tensile strength (UTS), the elongation, and the Young's modulus. For the EB-PVD aluminum tested at ambient temperature and an average strain rate of 4.0×10^{-4} s^{-1}, we obtained an average 0.2%

Table 3
Ambient-temperature (~23 °C) results for electrochemically deposited copper

	YS, MPa	UTS, MPa	Young's modulus, GPa	Elongation, %
	229	247	93	2.0
	217	234	75	1.6
	227	251	66	2.3
Average	224	244	78	2.0

Tests were conducted at an average strain rate of 3.8×10^{-5} s^{-1}.

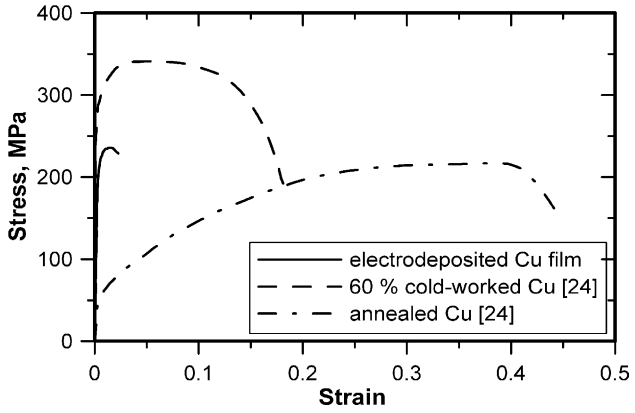

Fig. 8. Comparison of stress–strain behaviors of copper in different conditions. Our electrodeposited thin-film copper (thickness of 2.59 μm) exhibits small strain to failure compared to published results for bulk copper specimens (bar of 19 mm diameter).

offset yield strength of 94 MPa, with values ranging from 87 to 105 and an estimated standard deviation of 10.1 MPa. The average UTS was 151 MPa, with values ranging from 124 to 176 and an estimated standard deviation of 19.8 MPa. The average elongation was 22.5%, with values ranging from 13 to 32 and an estimated standard deviation of 5.0. The average Young's modulus was 27.8 GPa, with values ranging from 24.2 to 30.0 and an estimated standard deviation of 3.1 GPa. The observed Young's modulus is lower than the value for bulk pure aluminum [22]. This observation is consistent with reports of other researchers [4,7] that Young's modulus of thin-film aluminum is low. The obtained 0.2% offset yield strength and UTS are higher than those of bulk materials that is also consistent with other reports [4,7].

Table 1 shows the results obtained at ambient temperature (~23 °C) for polyimide (Specimen 2), along with the manufacturer's data [23]. The scatter in test results is within the range of typical tensile tests using large specimens. The agreement with manufacturer's data is excellent, especially the UTS. Table 2 lists the results obtained at elevated temperatures. The results show limited scatter even at elevated temperatures. We use the term "slope" in Table 2 instead of Young's modulus because the term "Young's modulus" is generally reserved for those elastic deformations that are associated with changes in interatomic spacing of crystals. The elastic deformation of the organic polyimide is different from the changes in interatomic spacing.

Table 3 shows the test results for the electrochemically deposited copper (Specimen 3). The tests were conducted at ambient temperature (~23 °C) and an average strain rate of 3.8×10^{-5} s^{-1}. The stress–strain curve of one of the specimens is plotted against those of the larger specimens under annealed and cold-worked conditions [24], as shown in Fig. 8. We observe that the strain to failure for the thin-film copper is very small even compared with that of the 60% cold-worked copper. The work-hardening behavior of the thin-film copper is similar to that of the 60% cold-worked copper. The work hardening is limited to a few percent of the initial loading, while annealed copper continues to work-harden to a strain of about 40%. Similar to EB-PVD aluminum, the observed Young's modulus in thin-film copper is also lower than that reported for the bulk materials [22].

9. Summary

A tensile-testing technique for testing thin films has been developed at the National Institute of Standards and Technology. The testing setup has loading displacement speeds ranging from 0.004 to 2 μm/s and force capacities in millinewtons. The force capacity of the setup can be changed depending upon the load requirement of a given test. The setup can test specimens from ambient temperature (~23 °C) to 200 °C.

Specimens are designed and fabricated using microfabrication techniques that are similar to those used in the semiconductor industry. The nominal dimension of a typical specimen is 180 μm × 10 μm × 1 μm.

While thin-film photodefinable polyimide shows properties similar to those reported by the manufacturer, EB-PVD thin-film pure aluminum and electrodeposited thin-film copper exhibit mechanical behaviors quite different from those of larger specimens. Generally, thin-film aluminum and copper have lower Young's moduli, smaller strains to failure, and higher yield strength and UTS. Thus, film properties cannot be extrapolated accurately from data obtained with large specimens. They need to be measured in the dimension and conditions existing in the structures or devices in which they are used.

References

[1] ASTM E8 Test Methods for Tension Testing of Metallic Materials, Annual Book of ASTM Standards, vol. 03.01, 2003.
[2] ASTM E8M Test Methods for Tension Testing of Metallic Materials (Metric), Annual Book of ASTM Standards, vol. 03.01, 2003.
[3] ASTM E345 Standard Test Methods of Tension Testing of Metallic Foil, Annual Book of ASTM Standards, vol. 03.01, 2003.
[4] R.W. Hoffman, in: J.C. Bravman, W.D. Nix, D.M. Barnett, D.A. Smith (Eds.), Proc. Materials Research Society Symposium, vol. 130, 1989, p. 295.
[5] R.W. Hoffman, in: G. Hass, R.E. Thun (Eds.), Physics of Thin Films, vol. 3, Academic Press, New York, 1966, p. 211.
[6] J.W. Menter, D.W. Pashley, in: C.A. Neugebauer, J.D. Newkirk, D.A. Vermilyea (Eds.), Proc. Structure and Properties of Thin Films, John Wiley Sons, Inc., New York, 1959, p. 111.
[7] J.E. Steinwall, Microfabrication and mechanical properties of free standing thin films, PhD Thesis, Cornell University, Ithaca, NY, 1992.
[8] T. Tsuchiya, J. Sakata, in: C.L. Muhlstein, S.B. Brown (Eds.), Mechanical Properties of Structural Films, ASTM STP 1413, American Society for Testing and Materials, West Conshohocken, PA, 2001, p. 214.
[9] I. Chasiotis, W.G. Knauss, Exp. Mech. 42 (2002) 51.

[10] S. Greek, S. Johansson, Micromach. Devices Compon III-SPIE 3224 (1997) 344.
[11] W.N. Sharpe Jr., K. Turner, R.L. Edwards, Proc. Material Research Society Symposium, vol. 518, 1998, p. 191.
[12] D.A. LaVan, K. Jackson, B. McKenzie, S.J. Glass, T.A. Friedmann, J.P. Sullivan, T.E. Buchheit, in: C. Muhlstein, S.B. Brown (Eds.), Mechanical Properties of Structural Films, ASTM STP 1413, American Society for Testing and Materials, West Conshohocken, PA, 2001, p. 62.
[13] D.T. Read, Y.W. Cheng, R.R. Keller, J.D. McColskey, Scr. Mater. 45 (2001) 583.
[14] W.C. Oliver, G.M. Pharr, J. Mater. Res. 7 (1992) 1564.
[15] A.J. Griffin Jr., F.R. Brotzen, C.F. Dunn, Thin Solid Films 150 (1987) 237.
[16] D.T. Read, J.D. McColskey, Y.W. Cheng, Proc. SEM Annual Conference on Experimental and Applied Mechanics, Portland, OR, June 4–6, 2001, p. 442.
[17] M.A. Sutton, J.L. Turner, H.A. Bruck, T.A. Chae, Exp. Mech. 31 (1991) 168.
[18] D.T. Read, Y.W. Cheng, M.A. Sutton, Proc. SEM Annual Conference on Experimental and Applied Mechanics, Portland, OR, June 4–6, 2001, p. 365.
[19] D.T. Read, Y.W. Cheng, J.D. McColskey, Proc. SEM Annual Conference on Experimental and Applied Mechanics, Milwaukee, WI, 2002, p. 64.
[20] Operating Manual, Burleigh Instruments, Inc. 1996.
[21] W.N. Sharpe Jr., Y. Bin, R. Vaidyanathan, Proc. IEEE, the Tenth Annual International Workshop on Micro Electro Mechanical Systems, Nagoya, Japan, IEEE, New York, NY, 1997, p. 424.
[22] Smithells Metals Reference Book, Paperback Edition, 7th edition, Butterworth-Heinemann, Oxford, UK, 1998.
[23] HD MicroSystems, Product Information and Process Guideline for Pyralin PI 2730 Series, July, 1998. The material used in the study is PI2737.
[24] Howard E. Boyer (Ed.), Atlas of Stress–Strain Curves, ASM International, Metals Park, OH, 2000.